Plasma Diagnostics in rf Discharges Using Nonlinear and Resonance Effects

Michael KLICK, Wolfgang REHAK and Marita KAMMEYER Adolf-Slaby-Institute, Rudower Chaussee 6a, D-12489 Berlin, Germany

(Received January 21, 1997; accepted for publication April 24, 1997)

In modelling rf discharges, nonlinear phenomena usually are treated as inconvenient effects. A method based on a nonlinear phenomenon is the self excited electron plasma resonance spectroscopy (SEERS). This new method for plasma monitoring allows to determine density and collision rate of the electrons and the power dissipated in the plasma body. Microwave interferometry (MWI) and Langmuir probe (LP) measurements were used to verify this method. This is shown for inert (He, Ar) and electronegative gases (O₂, CF₄). Examples of *in situ* control in plasma etching process are described. The high sensitivity and the capability of endpoint detection are shown.

KEYWORDS: plasma diagnostic, nonlinear phenomena, rf discharges, resonance effects, process control, process monitoring, plasma control

1. Introduction

The measurement of plasma parameters as density, collision rate and temperature of electrons, the power dissipated in the plasma body by electrons, provides important parameters for the characterization of the plasma, plasma sources, and modelling of discharges used for etching and deposition. A variety of techniques as Self Excited Electron Resonance Spectroscopy (SEERS), Langmuir Probe (LP), and Microwave Interferometrie (MWI) are available to determine plasma parameters. LP and MWI are well known methods and were often used for different plasmas. SEERS is a special method for cylindrical discharges with (also additional) capacitive rf excitation. Thus SEERS has to be verified comparing the results with independent diagnostic methods. Based on its unique properties concerning stability under real process conditions, it is utilized to show the correlation of plasma parameters (electron density and collision rate) and external parameters. Furthermore, SEERS is able to ensure stability and scaling of plasma processes in RIE, PE or PECVD systems.

2. Self Excited Electron Resonance Spectroscopy (SEERS)

Nonlinear phenomena in asymmetrical rf discharges are well known. A simple example is the bias voltage as a result of the rectification of the rf sheath voltage due to the nonlinear relation of sheath voltage and conduction current, particular the electron current. Also the occurence of harmonics in the discharge current is known but an exact theoretical treatment and measurement are difficult. Additional resonance effects in rf discharges are only reported recently.^{1–3)} It will be shown that a nonlinear resonance is a fundamental effect of the capacitive rf discharge and allows to determine essential plasma parameters.

Assuming a cylindrical and strong asymmetrical discharge and taking into account the electron density distribution within the sheath of the rf electrode, the occurrence of harmonics in the rf discharge can be investigated. Because of the inertia of the bulk electrons these harmonics excite oscillations in the discharge at the geometric resonance frequency located below the plasma resonance frequency.^{1–4} Similar effects are known as main

resonance of the Tonks-Dattner-resonances,^{5–9)} using an external excitation of (resonance) probes¹⁰⁾ or resonant rf discharges.^{11,12)}

For rf frequencies well above the ion plasma frequency, $\omega \gg \omega_{\rm i}$, the ions cannot respond to the fast variations of the electric field. The ion and electron plasma frequency (Langmuir frequency) is defined by $\omega_{\rm e,i}=(n_{\rm e,i}e^2/m_{\rm e,i}\varepsilon_0)^{1/2}$, where $m_{\rm e,i}$ denotes the electron or ion mass, e its charge, and ε_0 and $n_{\rm e,i}$ the permittivity of the free space and the electron or ion density, respectively. Therefore the ion density depends only on the time averaged electric field and is not a function in time. Since $\omega_{\rm i}^{-1}$ is, at least for the rf discharge, less than the time constant of the ambipolar diffusion, the plasma density can be assumed to be independent of time. $^{13-15)}$ Usually the plasma density is sufficiently high so that the Debye length

$$\lambda_{\rm D} = \left(\frac{\varepsilon_0 k T_{\rm e}}{n_{\rm e} e^2}\right)^{1/2} \ll L, \ R \tag{1}$$

and, respectively, for moderate sheath voltages, also the sheath width are significantly less than electrode gap and radius R for any ion density n_i within the plasma body.

In order to investigate the plasma body only the range between the ion and electron plasma frequency

$$\omega_{\rm i} \ll \omega \ll \omega_{\rm e}$$
 (2)

is considered. Particularly for $\omega_{\rm e}$, this condition has to be satisfied for any electron density $n_{\rm e}$ within the plasma body. Because of the last two assumptions, kinetic effects, wave propagation, and local resonances play no role and the well known hydrodynamic approach (cold plasma approximation) can be used. $^{5,7-9,16,17)}$ It involves electron collisions by the constant collision rate $\nu_{\rm e}$ and results in the permittivity ε of an isotropic plasma

$$\frac{\varepsilon}{\varepsilon_0} = 1 - \frac{\omega_e^2}{\omega(\omega - i\nu_e)}.$$
 (3)

Since a rf resonance is treated only, displacement D, electric field E and potential φ were considered without dc part. They meet, e.g., ¹⁸⁾

$$\nabla D = \nabla \cdot (\varepsilon E) = \varepsilon \nabla \cdot E + E \cdot \nabla \varepsilon = 0, \tag{4}$$

and for a weakly inhomogenous plasma body

$$\left| \frac{\nabla E}{E} \right| \gg \left| \frac{\nabla \varepsilon}{\varepsilon} \right| \approx \left| \frac{\nabla n_{\rm e}}{n_{\rm e}} \right|,$$
 (5)

one can approximate ε by its reciprocally averaged value, analogeous to the exact result of the one-dimensional case,⁹⁾

$$\tilde{\varepsilon} = \left(\frac{1}{V} \int_{V} \varepsilon^{-1} \, \mathrm{d}V\right)^{-1} \tag{6}$$

and obtains finally the Poisson equation for the rf potential φ . Taking into account the boundary conditions in cylinder coordinates, the above equation can be written as¹⁹)

$$\frac{\partial^2 \varphi}{\mathrm{d}r^2} + \frac{1}{r} \frac{\partial \varphi}{\mathrm{d}r} + \frac{\partial^2 \varphi}{\mathrm{d}z^2} = 0, \tag{7}$$

which has, for finite potential φ at r=0, the series solution¹⁹⁾

$$\varphi(r, z) = \sum_{k} J_0(kr) (A_k \cosh kz + B_k \sinh kz), \quad (8)$$

where J_0 denotes the Bessel function of first kind and zero order. This type of solution are well known from the theory of ambipolar diffusion for the density distribution in cylindrical systems, $^{20,21)}$ but the boundary conditions are completely different in this case. The eigenvalues k and the unkown coefficients B_k have to be determined from the boundary conditions shown in Fig. 1. R and $R_{\rm E}$ are the radii of the vacuum chamber and the rf electrode, respectively. L is the length of the plasma body.

Because of the area ratio, the potential drop of the sheath at the wall is usually much smaller than the sheath voltage at the driven electrode. In agreement to modeling and experimental experience, this results, particular concerning the ratio of bias and peak voltage, in the thickness ratio $s \gg s_{\rm w}$. Thus the sheath at the wall can be neglected for the approach used here and the boundary conditions can be simplified so that the potential equals zero at the conducting wall

$$\varphi(r, 0) = V_{\rm p}, r < R_{\rm E}$$

$$\varphi(r, 0) = 0, R_{\rm E} < r \le R$$

$$\varphi(r, L) = 0, r \le R$$

$$\varphi(R, z) = 0, z \le L.$$
(9)

Now there is only one region and no separate treatment and matching is necessary.

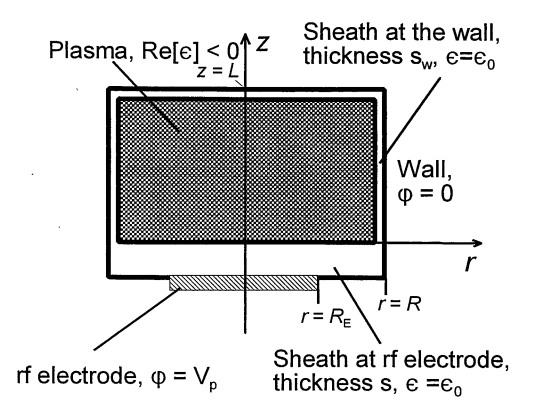


Fig. 1. Boundary conditions of the cylindrical rf discharge.

Using the substitution y = z - L, the A_k vanish owing to the boundary condition at z = L (y = 0). The boundary condition at z = 0 (y = L) can be expanded into a Fourier-Bessel-series.¹⁹⁾ The comparism of the coefficients in eq. (11) provides the unknown B_k and results in

$$\varphi(r, y) = 2V_{p} \frac{R_{E}}{R} \sum_{k} \frac{J_{1}\left(\xi_{k} \frac{R_{E}}{R}\right)}{\xi_{k} J_{1}^{2}(\xi_{k}) \sinh\left(\xi_{k} \frac{L}{R}\right)} \times \sinh\left(\xi_{k} \frac{y}{R}\right) J_{0}\left(\xi_{k} \frac{r}{R}\right), \tag{10}$$

 ξ_k denotes the zeros of J_0 . The derivative of the potential with respect to y at z=0 (y=L) in the above equation shows that the field has a singularity by reason of the jump of φ at $R_{\rm E}$. This is, basically, the consequence of the unphysical boundary condition which is contrary to the finite conductivity of the plasma body. In order to remove this singularity, the higher eigenvalues are neglected keeping φ at r=0, z=0 constant ($\varphi=V_{\rm p}$).

Since the permittivity of the plasma is given, the solution (10) of the partial differential eq. (7) results in a total current, using $j(r, y) = -\mathrm{i}\omega\varepsilon E(r, y)$ for the local current density, and an (complex) impedance of the plasma body. In order to get a complete one-dimensional model, we introduce the effective length of the plasma body as the length of a cylindrical plasma body with the diameter $R_{\rm E}$ the same total current. This yields, in agreement to a numerical solution, the approximation for the effective length of the plasma body^{2,24}

$$\dot{l} = \frac{R}{x_0} \tanh \frac{x_0 L}{R} \,, \tag{11}$$

 $x_0=2.405$ is the first zero of the Bessel function (comp. eq. (11)). This result is correct for $L\ll R/2$ ($l\approx L$) or $R\approx 1.5R_{\rm E}$ and otherwise a good approximation. For $L\gg R/2$ one obtains $l\approx R/x_0$. That can readily understood, in order to obtain the effective length of l of the plasma body the radial and axial current has to be taken into account. For $z\gg R/2$ rf potential and current are very small and this part of the plasma body plays no role concerning the whole current. Finally, we obtain for the impedance of the plasma body

$$Z = \frac{m_e l}{\tilde{n}e^2 \pi R_F^2} (i\omega + \nu)$$
 (12)

consisting of a resistive and an inductive part. The volume averaged electron density can, for $(\omega_e/\omega)^2 \gg 1 + (\nu/\omega)^2$, be derived from eq. (6)

$$\tilde{n} = \left(\frac{1}{V} \int_{V} n_{\rm e}^{-1} \,\mathrm{d}V\right)^{-1}.\tag{13}$$

After the treating behavior of the plasma body (bulk), one has to analyse the nonlinear effect providing harmonics. For the one-dimensional analysis of the rf sheath we introduce the dimensionless quantities

$$\zeta_{\rm e} = \frac{n_{\rm e}}{n_{\rm o}}, \quad \zeta_{+} = \frac{n_{+}}{n_{\rm o}}, \quad \eta = \frac{V_{\rm o} - V}{kT_{\rm e}/e},$$

$$\xi = \frac{z_{\rm o} - z}{\lambda_{\rm Do}}, \quad \tau = \omega_{\rm rf}t, \tag{14}$$

normalizing the electron and ion densities $n_{\rm e,i}$ with the plasma density close to sheath edge $n_0=n(r,z_0)$, the potential V with the (thermal) electron energy $kT_{\rm e}$, the space coordinate z with the Debye length $\lambda_{\rm D0}$ at n_0 . The plasma density n_0 and the electron temperature $T_{\rm e}$ are supposed to be constant. τ denotes the normalized time. The ions can respond only to the time averaged electric field. Thus we define z_0 ($\xi=0$) on the one-dimensional scale of the sheath to be the point where the Bohm criterion is satisfied.

The displacement current $j_{\rm d}$ is expressed in units of the electron saturation current $j_{\rm es}$

$$\Gamma_{\rm d} = \frac{j_{\rm d}}{j_{\rm es}(2\pi)^{1/2}},$$

$$(2\pi)^{1/2}j_{\rm es} = en_0\lambda_{\rm D}\omega_{\rm e} = en_0\left(\frac{kT_{\rm e}}{m_{\rm e}}\right)^{1/2}.$$
(15)

The relation between (normalized) displacement current $\Gamma_{\rm d}$, sheath voltage $\eta_{\rm s}$, and sheath width δ can now be written in the time domain as⁴)

$$\Gamma_{\rm d} = \frac{\Omega}{\delta(\eta_{\rm s})} \frac{\mathrm{d}\eta_{\rm s}}{\mathrm{d}\tau} \,,\tag{16}$$

which is a fundamental relation without any direct dependence on the density distributions $\xi_{e,+}$. In ref. 4 this relation is found to be not bounded on a step-wise electron density if a generalized definition of the time dependent sheath boundary is used.

We introduce the normalized coefficients for the plasma body

$$\Lambda = \frac{n_0}{\tilde{n}} \frac{l}{\lambda_D} \frac{\omega_{\rm rf}}{\omega_{\rm e}} \,, \quad \rho = \frac{n_0}{\tilde{n}} \frac{l}{\lambda_D} \frac{\nu_{\rm e}}{\omega_{\rm e}} \,, \quad (n_{\rm e} = \tilde{n}), \tag{17}$$

where ν_e the electron collision rate again. Using eq. (12), the potential drop of the plasma can now be written in the frequency domain as

$$\eta_{\rm p} = i\mu\Lambda\Gamma + \rho\Gamma,\tag{18}$$

i μ is the operator resulting from the Fourier transformation, $\mu = \omega/\omega_{\rm rf}$ is the normalized frequency being integer for the harmonics of $\omega_{\rm rf}$. Neglecting the thin sheath at the grounded electrode, see eq. (9), the total discharge voltage can be expressed as $\eta_{\rm rf} = \eta_{\rm s} + \eta_{\rm p}$ and we obtain for the whole rf discharge the following set of two coupled first order, non-linear differential equations for sheath voltage and discharge current²⁾ or in the frequency domain ($\Omega = \omega_{\rm rf}/\omega_{\rm e}$)

$$i\mu\eta_{\rm rf} = \Omega^{-1}\delta * \Gamma + i\mu\rho\Gamma - \mu^2\Lambda\Gamma,\tag{19}$$

where * denotes the convolution and involves the non-linear excitation. Note that δ depends on the sheath potential. In agreement with a theoretical estimation⁴⁾ and experimental results,²⁾ the convection current, ion and electron current in the sheath, can be neglected $(\Gamma = \Gamma_d)$. In order to calculate the discharge current a sinusoidal voltage at the rf electrode

$$\eta_{\rm rf}(\tau) = \hat{\eta}\sin\tau + \eta_{\rm B},\tag{20}$$

is assumed, $\eta_{\rm B}$ is the (self) bias voltage. This approach was verified in ref. 4.

Taking into account the capacitive behavior of the

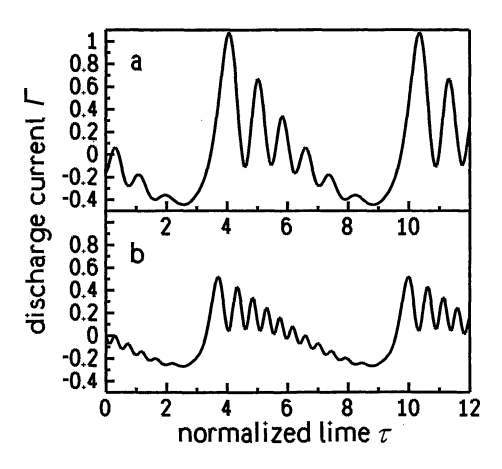


Fig. 2. Discharge current, ref. 2, $\hat{\eta} = 100$, $\eta_{\rm B} = 105$, a) $\Omega = 0.05$, $\rho = 8$, $\Lambda = 6$; b) $\Omega = 0.03$, $\rho = 4$, $\Lambda = 3$.

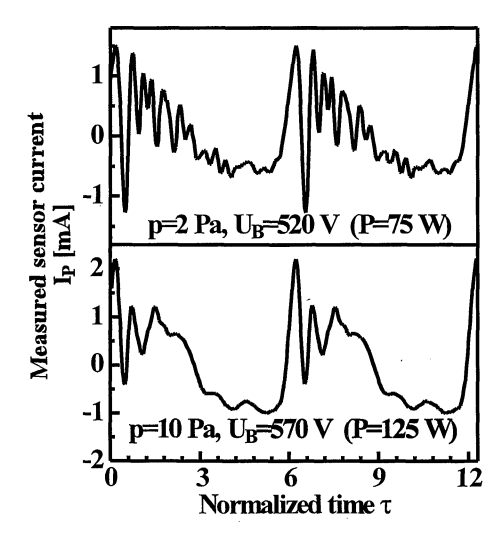


Fig. 3. Measured part of the discharge current in Ar (see Fig. 4).

sheath, the discharge can be regarded as a damped oscillation circuit. The nonlinear sheath "capacitance", see eq. (16), excites the plasma by providing harmonics causing damped oscillations close to the geometric resonance frequency,²⁾ which is located below the plasma frequency. For asymmetrical discharges and sinusoidal voltage, the current can be shown to consist of a saw tooth shaped part (nonlinearity) and a superposed damped oscillation. A numerical solution of eqs. (19) and (20), assuming a homogeneous ion density distribution within the sheath, was given in ref. 2 and is shown in Fig. 2. The sheath thickness δ was calculated in terms of the displacement D by integrating Γ .⁴⁾ The assumption of homogeneous ion density provides $\delta \propto D$.

A rough approximation for the resonance or, strictly speaking, the eigenfrequency can, in case of low damping and using timely averaged sheath thickness \bar{s} , be derived from eq. $(19)^{2,12}$

$$\omega_0 \approx \left(\frac{\bar{s}}{l}\right)^{\frac{1}{2}} \omega_e = \left(\frac{\bar{s}}{l} \frac{\tilde{n}e^2}{m_e \varepsilon_0}\right)^{\frac{1}{2}}.$$
 (21)

Generally, a characteristic eigenfrequency ω_0 can be defined by the additional condition that the displacment D, or the field E, equals its averaged value $D = \bar{D}$.

This results also in a 'electrical' sheath thickness which replaces \bar{s} in the above equation and was used for the frequency $f_0 = \omega_0/2\pi$ in Fig. 6.

When the discharge current was measured, a least squares fitting (maximum likelihood estimation)

$$\sum_{\mu} \left| \Omega^{-1} \delta * \left(\frac{K_{\mathrm{p}} I_{\mathrm{p}}}{(2\pi)^{1/2} j_{\mathrm{es}}} \right) + (\mathrm{i}\mu \rho - \mu^{2} \Lambda) \left(\frac{K_{\mathrm{p}} I_{\mathrm{p}}}{(2\pi)^{1/2} j_{\mathrm{es}}} \right) - \mathrm{i}\mu \eta_{\mathrm{rf}} \right|^{2} \to \min$$

$$(22)$$

provides the unknown coefficients ρ and Λ in eq. (19) and the ratio between the true discharge current and the current from the sensor K_p which was assumed to be independent of μ . From these normalized coefficients one can derive the averaged electron plasma density defined by eq. (13), the electron collision rate, the plasma resistance and other important plasma parameter as the bulk power.^{2,25)}

Two different measurements of the discharge current, strictly speaking a part of the current, using a sensor flat in the wall, are shown in Fig. 3. (see experimental setup). As expected, the predicted oscillations in the discharge current are well pronounced and the damping increases at higher pressure.

3. Experimental Setup

Because of unavoidable stray and feedthrough capacitances at the powered electrode, a direct measurement of the discharge current is very difficult in commercial systems. SEERS uses a special sensor in a coaxial geometry $(50\,\Omega)$ inserted into the wall (flange) of the recipient as a virtual part of the wall. By means of the nonlinear model, the current pitch ratio of the current measured and the real discharge current can be determined. Therefore, calibration depending on the sensor position is not necessary.

The discharge current is detected by a digital sampling oscilloscope HP $54616B~(500\,\mathrm{MHz}, 2\,\mathrm{GS/s})$ and the cor-

responding parameters are processed by a fast numerical algorithm. Using the differential equation and the measured discharge current, the unknown coefficients can be determined.

For the experimental comparism with Langmuir probe measurements, a commercial RIE system was used (Alcatel GIR 300). As can be seen in Fig. 4, the chamber comprises a driven substrate electrode and a grounded upper electrode in a cylindrical vessel. The lower electrode was powered at 13.56 MHz. The diameter of electrodes and chamber was 15.5 cm and 30 cm, respectively. The electrode gap was 6.7 cm. The details were described in ref. 25.

The experiments were carried out in inert (Ar) and electronegative gases (O_2, CF_4) at a pressures of $2\,\mathrm{Pa}$. The sensor for the discharge current measurement (SEERS) and the Langmuir probe (LP) were mounted in KF 40 flanges. The position of the Langmuir probe tip was between the electrodes at a radius of 12 cm with a distance of 3 cm to the grounded, upper electrode. The Langmuir probe system from the Munich University of Technology used a tungsten wire with 8 mm length and a diameter of $100\,\mu\mathrm{m}$ as the probe tip.

The comparison of MWI and SEERS (see Fig. 5) was performed in special chamber with quartz ring (diameter 21 cm). In order to keep the discharge asymmetrical and to minimize the influence of the quartz wall, the gap of electrodes (4 cm) and the rf electrode (diameter 4 cm) were small.

4. Experimental Results

For the experiments a bias voltage (power) was varied in Ar, O₂, and CF₄. The range around 2 Pa ensures a sufficiently homogenous plasma. Therefore the Langmuir probe measurement (LP), providing local values of the electron density, can be compared with SEERS, yielding averaged values, see eq. (13).

At first, the basic effect should be illustrated discussing the dependence of the resonance frequency on external

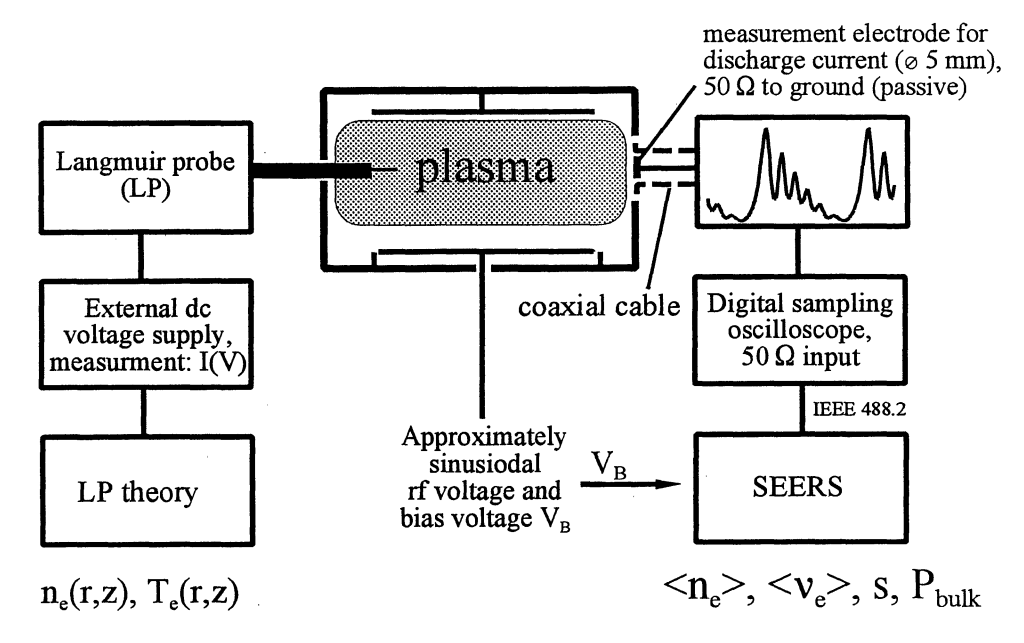


Fig. 4. Experimental setup of Langmuir probe and SEERS.

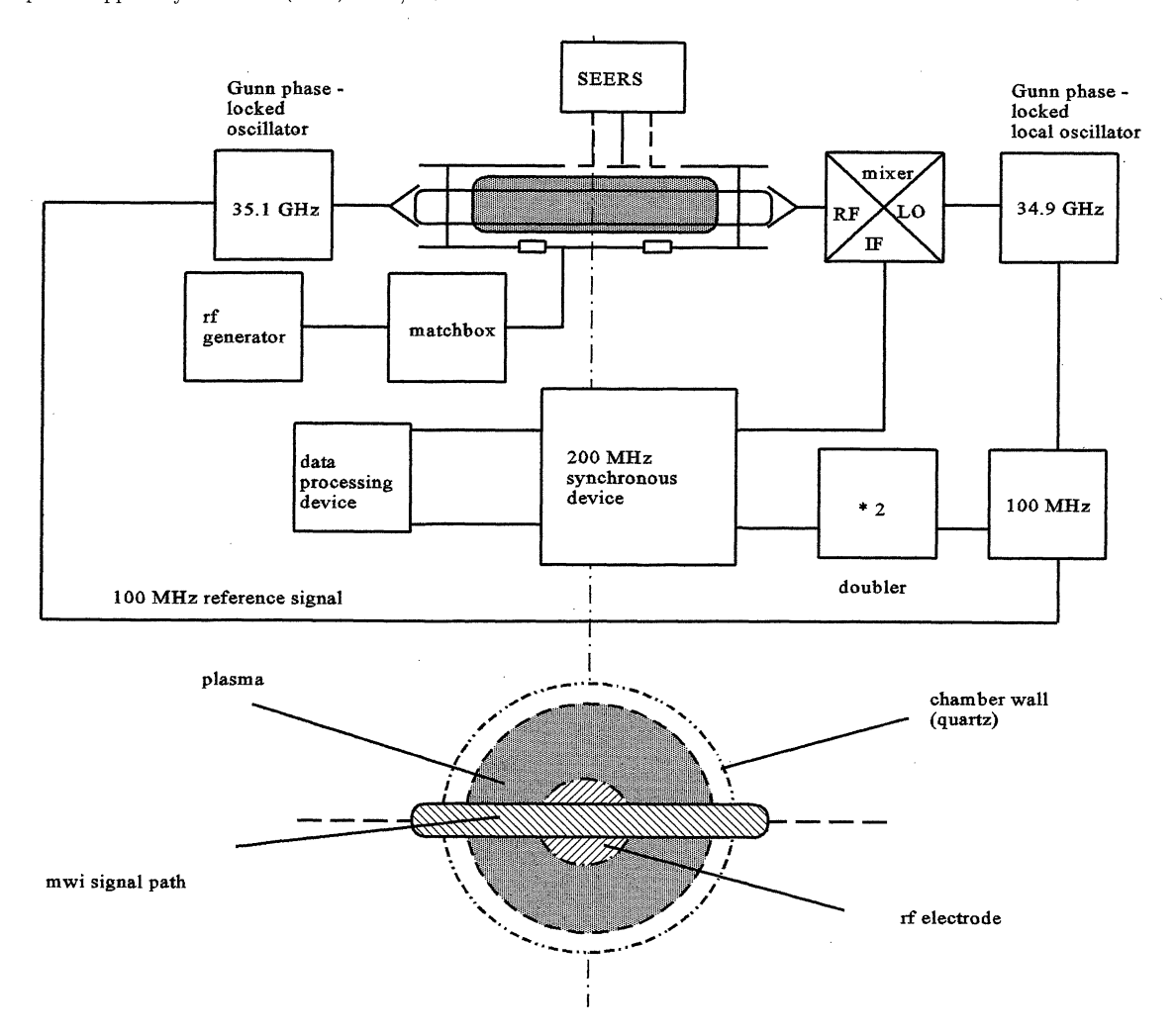


Fig. 5. Special experimental setup of Microwave interferometry and SEERS.

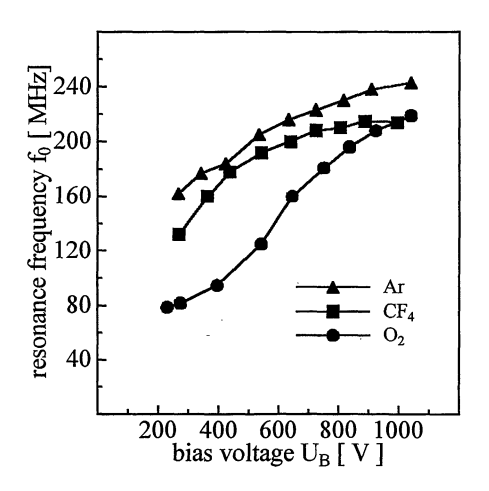


Fig. 6. Resonance frequency vs. bias voltage.

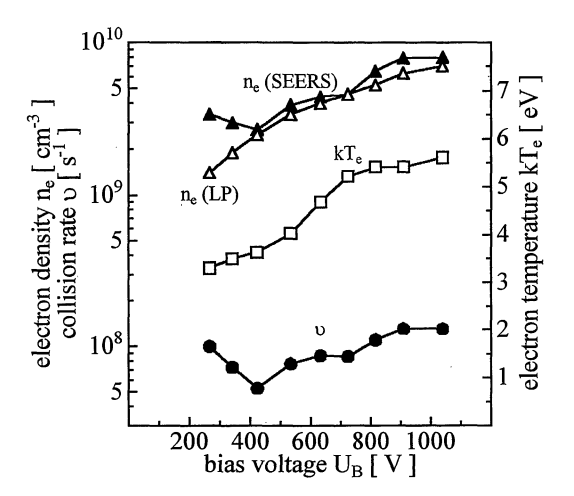


Fig. 7. Density, collision rate, and temperature of electrons vs. bias voltage in Ar.

discharge parameters. As expected, the resonance frequency increases if power or bias voltage is increased. This can readily be understood bearing in mind that an increasing power leads to a higher density causing an increase of the retarding field within the rf sheath.

Figure 6 shows the influence of gas type on the dependence of the resonance frequency. Notice that, in contrast to linear systems, the resonance frequency timely

varies. Thus, the resonance frequency is defined by the additional condition that the field at the rf electrode equals its average value.

The lower frequencies for O₂ indicates a lower electron density, comp. Fig. 8. For the experimental conditions used here, the resonance frequency is located around the 10th harmonics, generally between the 3th and 25th har-

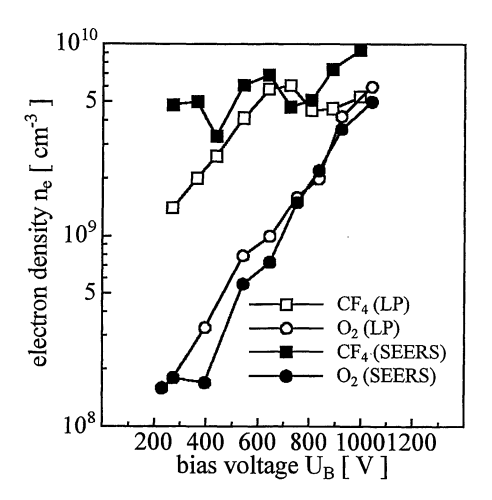


Fig. 8. Electron density vs. bias voltage for O2 and CF4.

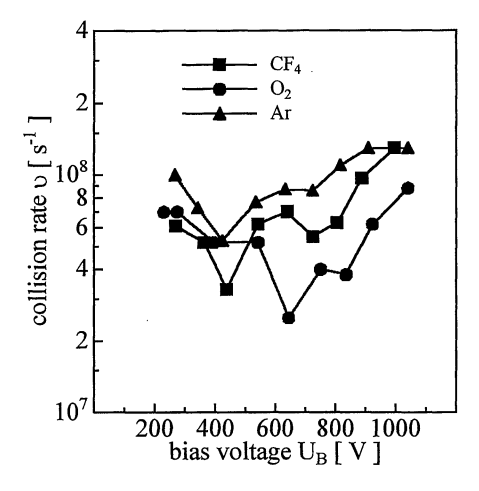


Fig. 9. Collision rate vs. bias voltage for different gases.

monics.

Figure 7 shows the density, temperature, and collision rate of the bulk electrons in Ar at 2 Pa from ref. 25. Both independent methods show a good agreement for the electron density values, the increase of the collision rate is owing to the stronger field within the plasma body resulting in a higher electron temperature as well.

Being independent of gas type, SEERS can easily extented to the electronegative gases. Figure 8 presents the electron densities in O_2 and CF_4 . For oxygen, one obtains a good agreement between both methodes. For CF_4 , which is much more complex because of the high fragmentation, the discharge is slightly less stable yielding an increased error of both methodes. A second known reason is the rising density of negative ions resulting in a different axial density profile in the bulk plasma of CF_4 .

The collision rate is calculated from the damping constant of the measured oscillations and is compared for Ar, O₂ and CF₄ at 2 Pa in Fig. 9. The dependence of the collision rate on the bias voltage requires further discussion. The high collision rate for Ar appears due to charge transfer collisions resulting in a large effective cross section. This predicts also a higher bulk power of the Ar discharge, as can be seen in Fig. 10.

For the microwave interferometry, a higher pressure

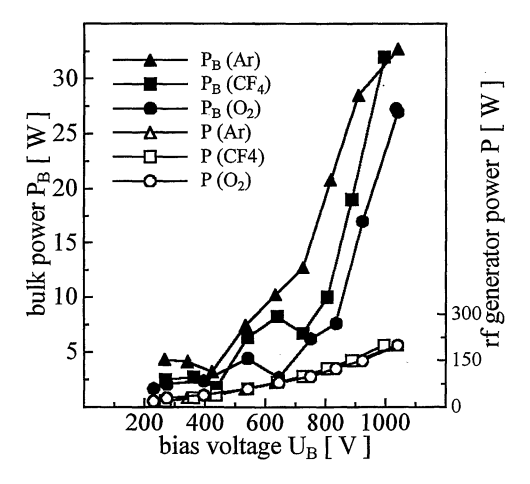


Fig. 10. Bulk and generator power vs. bias voltage for different gases.

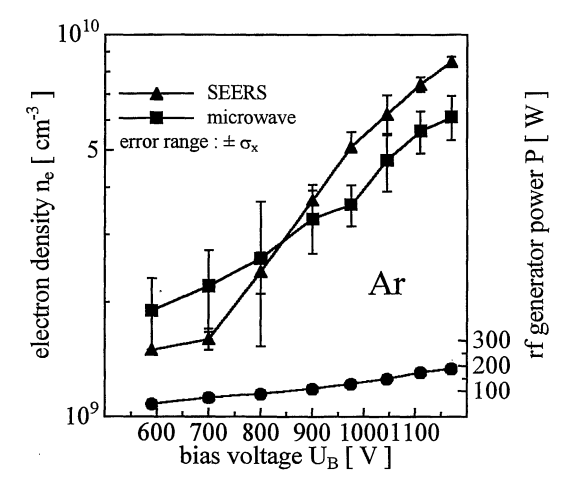


Fig. 11. Comparism of electron densities from SEERS and MWI vs. bias voltage in Ar.

(10 Pa) was required for sufficient discharge stability. The different kind of averaging of SEERS and MWI ($\lambda=8\,\mathrm{mm}$) predicts, a deviation between both methodes. It should be noted that the average electron density determined by MWI is averaged along the path of the microwave signal through the plasma. The electron density from MWI was calculated from the phase shift of the microwave signal, see experimental setup and ref. 26. The lower drawing in Fig. 5 demonstrates that the weak part of the bulk, far away from the small rf electrode, will decrease the averaged density delivered by SEERS in comparism to the MWI value. Fortunately, this effect is only weak pronounced and both systems provide approximately the same values for the electron density. This is shown for Ar and O2 in Figs. 11 and 12.

5. Application

Figure 13 demonstrates an example for the etching of poly-Si/SiO₂/Si with HI-chemistry. Contrary to the bias voltage, the electron density depends strongly on plasma physics and chemistry and indicates also slight changes of process conditions. Because of the sensitive responds of SEERS plasma parameters on reactor changes, the

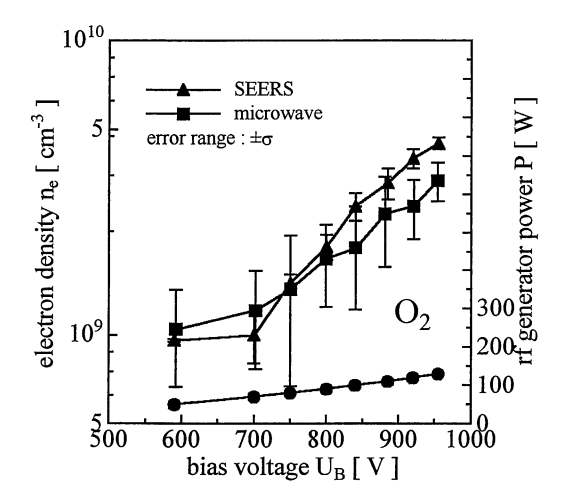


Fig. 12. Comparism of electron densities from SEERS and MWI vs. bias voltage in O₂.

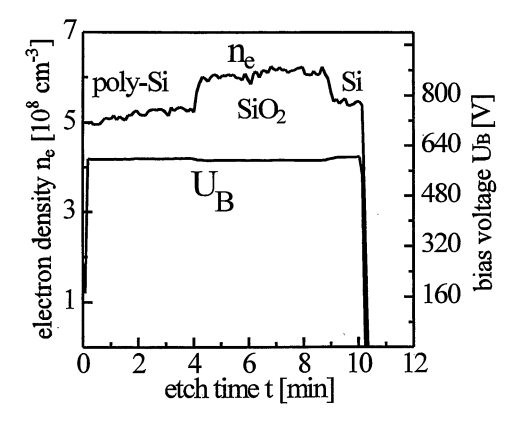


Fig. 13. Gate etching (poly-Si/SiO $_2/Si)$ in SiCl $_4/Cl_2/N_2;$ 250 W; 13.56 MHz; 5 Pa.

monitoring system is suitable to define the chamber condition exactly and reproducibly,²⁷⁾ an extention to high density plasma appears to be possible.²⁸⁾ The control and monitoring of plasma properties during dry etching and deposition processes remains integral in microelectronic technology. This process control of semiconductor manufacturing is of crucial economic importance.

Acknowledgements

The authors thank Dr. W. Kasper and Dr. P. Awakowicz, Munich University of Technology, and Dr. G. Franz, Siemens AG Munich, for experimental data. The authors are also grateful to S. Fujii for valuable comments

and H. Mischke, D. Suchland and L. Eichhorn for helpful discussions.

- 1) M. Klick: German patent application DE-A-4445762, 1994.
- M. Klick and W. Rehak: 12th Int. Symp. Plasma Chemistry, Minneapolis, USA, 1995, Vol. 1, pp. 511-516.
- B. M. Annaratone, V. P. T. Ku and J. E. Allen: J. Appl. Phys. 77 (1995) 5455.
- 4) M. Klick: J. Appl. Phys. 79 (1996) 3445.
- 5) I. Langmuir and L. Tonks: Phys. Rev. 33 (1929) 195.
- 6) D. Bohm and E. P. Gross: Phys. Rev. 75 (1949) 1851.
- 7) E. Åström: Arkiv för Fysik 19 (1961) 163.
- 8) P. E. M. Vandenplas and R. W. Gould: Physica 28 (1962) 357.
- S. Wolschke: Ergebnisse der Plasmaphysik und der Gaselektronik Vol. III, ed. R. Rompe and M. Steenbeck (Akademie-Verlag, Berlin, 1972), pp. 175-251.
- R. S. Harp and F. W. Crawford: J. Appl. Phys. 35 (1964) 3436.
- 11) F. Schneider: Z. Angew. Phys. 6 (1954) 456.
- V. A. Godyak and O. A. Popov: Sov. J. Plasma Phys. 5 (1979) 277.
- V. E. Golant, A. P. Zhilinsky and I. E. Sakharov: Fundamentals of Plasma Physics (Wiley, New York, 1980) pp. 222-226.
- 14) M. Klick: Phys. Rev. E 1 (1993) 591.
- H. R. Snyder and C. B. Fleddermann: J. Appl. Phys. 73 (1993) 1001.
- 16) R. N. Franklin: Plasma Phenomena in Gas Discharges (Clarendon Press, Oxford, 1976) pp. 112–116.
- 17) J. C. Nickel, J. V. Parker and R. W. Gould: Phys. Rev. Lett. 11 (1963) 183.
- 18) J. H. Malmberg and C. B. Wharton: Phys. Rev. Lett. 4 (1996) 175
- P. Moon and D. E. Spencer: Field Theory Handbook (Springer-Verlag, Berlin, 1961) pp. 14, 185.
- V. A. Godyak and A. S. Kanneh: IEEE Trans. Plasma. Sci. 14 (1986) 112.
- M. A. Lieberman and S. E. Savas: J. Vac. Sci. Technol. A 8 (1990) 1632.
- 22) C. M. Horwitz: J. Vac. Sci. Technol. A 1 (1983) 60.
- 23) M. V. Alves, M. A. Lieberman, V. Vahedi and C. K. Birdsall: J. Appl. Phys. 69 (1991) 3823.
- 24) M. Klick: unpublished.
- 25) M. Klick, M. Kammeyer, W. Rehak, W. Kasper, P. Awakowicz and G. Franz: 5th Int. Conf. Plasma Surface Engineering, Garmisch-Partenkirchen, Germany, 1996.
- O. Auciello and D. L. Flamm: Plasma Diagnostics (Academic press, London, 1989) p. 247.
- 27) M.-A. Aminpur, H.-H. Richter, A. Wolff, D. Krófcger, A. Dehoff and M. Reetz: 3rd Int. Conf. Reactive Plasmas and 14th Symposium on Plasma Processing and 14th Symposium on Plasma Processing, Nara, Japan, 1997 (to be published in Jpn. J. Appl. Phys. 36 (1997) No. 7B).
- 28) Y. Sawa, H. Shindo, S. Fujii and Y. Horiike: 3rd Int. Conf. Reactive Plasmas and 14th Symposium on Plasma Processing and 14th Symposium on Plasma Processing, Nara, Japan, 1997 (to be published in Jpn. J. Appl. Phys. 36 (1997) No. 7B).